



ELSEVIER

Polymer 44 (2003) 883–894

polymerwww.elsevier.com/locate/polymer

A reactive molecular dynamics model of thermal decomposition in polymers: I. Poly(methyl methacrylate)

Stanislav I. Stoliarov^a, Phillip R. Westmoreland^a, Marc R. Nyden^{b,*}, Glenn P. Forney^b^aDepartment of Chemical Engineering, University of Massachusetts Amherst, Amherst, MA 01003-9303, USA^bBuilding and Fire Research Laboratory, National Institute of Standards and Technology, 100 Bureau Drive, Gaithersburg, MD 208998665, USA

Received 31 August 2002; received in revised form 18 October 2002; accepted 19 October 2002

Abstract

The theory and implementation of reactive molecular dynamics (RMD) are presented. The capabilities of RMD and its potential use as a tool for investigating the mechanisms of thermal transformations in materials are demonstrated by presenting results from simulations of the thermal degradation of poly(methyl methacrylate) (PMMA). While it is known that depolymerization must be the major decomposition channel for PMMA, there are unanswered questions about the nature of the initiation reaction and the relative reactivities of the tertiary and primary radicals formed in the degradation process. The results of our RMD simulations, performed directly in the condensed phase, are consistent with available experimental information. They also provide new insights into the mechanism of the thermally induced conversion of this polymer into its constituent monomers.

© 2002 Elsevier Science Ltd. All rights reserved.

Keywords: Reactive molecular dynamics; Poly(methyl methacrylate); Thermal decomposition

1. Introduction

Considerable effort has been directed towards understanding the mechanisms of chemical transformations in complex multi-component systems. For example, scientists have been able to resolve the combustion of gaseous fuels and chemical processes in the earth's atmosphere in terms of elementary chemical reactions with defined kinetic parameters [1,2]. Although the quantitative kinetic models are still far from being perfect, our knowledge of the underlying gas-phase chemistry has reached the point where it can be used to make realistic predictions of the behavior of such systems. Our understanding of the complex processes that govern the chemistry of the condensed-phase systems, however, is not so well developed.

Thermal degradation of polymers and polymer composites is one area, in particular, where knowledge of the underlying chemical mechanisms is insufficient to make accurate quantitative predictions. Experimental information is usually limited to data obtained from thermogravimetric analyses (TGA) or TGA in conjunction with mass

spectrometry (TGA/MS), which can only provide rate constants for the kinetics of the overall mass loss and yields of the final gaseous products. Statistical reaction rate theories (together with quantum chemical calculations of potential energy surfaces) have been quite successful when used to predict the rate constants of elementary reactions in the gas phase. However, they are not directly applicable to condensed-phase environments because of the absence of a consistent and physically realistic method for handling the coupling between all of the degrees of freedom. At the same time, the need to develop a molecular-level understanding of the thermal degradation of polymers is becoming increasingly important in areas of science and technology associated with the high-temperature processing and combustion of these materials.

The present work presents and employs an extension of classical force-field-based molecular dynamics to modeling chemical reactions that may be called reactive molecular dynamics (RMD). Quantum molecular dynamics methods, in which the classical dynamics of atomic structures is governed by forces obtained from quantum calculations [3], offer another option. The problem with application of the latter approach, however, is that the computational requirements necessary to obtain the accuracy required for the

* Corresponding author. Tel.: +1-301-9756692; fax: +1-301-9754052.
E-mail address: marc.nyden@nist.gov (M.R. Nyden).

prediction of rate constants would be prohibitive. Indeed, current applications of the Car–Parrinello method [4] to molecular solids using plane-wave expansions of the Kohn–Sham orbitals and gradient-corrected density functionals, which are still not adequate for a quantitative description of chemical reactions involving the dissociation and formation of covalent bonds, are already at the cutting edge of modern computational capabilities [3].

In our implementation of RMD, we use a computer program hereafter referred to as MD_REACT. MD_REACT was developed for investigating the thermal decomposition of polymeric materials. Earlier versions of this program have been successfully applied in studies of the mechanisms of thermal degradation in a number of simple polymers and polymer composites [5–7]. In Section 2 of this paper, we provide a summary of recent enhancements to the RMD approach, which we believe to be a further step forward in the development of a versatile computational tool for analysis of chemical processes in the condensed phase. Results of the application of the new version of MD_REACT to the thermal decomposition of poly(methyl methacrylate) (PMMA) are reported in Section 3.

The thermal degradation of PMMA has been the subject of numerous publications [8–15] and is considered to be a well-studied process. While it is known that PMMA depolymerizes almost exclusively to the monomer when heated, there are still unanswered questions about the nature of the initiation reaction and the relative reactivities of the primary and tertiary radicals formed in the degradation process. The results of our simulations provide new insights that may be helpful in resolving these issues. At the same time, these results indicate that there are some aspects of the thermal decomposition of large molecules in condensed phases that cannot be explained within the framework of traditional models of chemical reactivity, which were derived from analyses of the kinetics of small molecules in the gas phase.

2. Description of the RMD method

2.1. Principles and algorithm

The basis of RMD is solving the classical equations of motion for the atoms of the molecular system under study. The feature that distinguishes RMD from other force-field-based implementations of molecular dynamics is that covalent bonds between atoms are allowed to break and form during the course of the simulations.

In this method, atomic trajectories are computed by numerical integration of Hamilton's equations of motion

$$\frac{\partial H}{\partial p_i} = \frac{\partial q_i}{\partial t} \quad \frac{\partial H}{\partial q_i} = -\frac{\partial p_i}{\partial t}, \quad (1)$$

where q_i and p_i are the coordinates and components of momenta of the atoms, and t is time. The classical

Hamiltonian,

$$H = \sum_j^N \frac{\mathbf{p}_j^2}{2m_j} + V(q_1, q_2, \dots, q_{3N}), \quad (2)$$

is a mathematical expression for the sum of the kinetic and potential (V) energies associated with atomic motion. In Eq. (2), N is the number of atoms in the system; \mathbf{p}_j and m_j are the momentum vectors and masses of the atoms. In our present implementation, the potential energy is a modified form of the consistent valence force field (CVFF) [16]. It is summarized by Eq. (3)

$$V = \sum^{n_{\text{bonds}}} V_{\text{bond}} + \sum^{n_{\text{angles}}} V_{\text{angle}} + \sum^{n_{\text{torisons}}} V_{\text{torisons}} + \sum^{n_{\text{pairs}}} V_{\text{nonbond}}. \quad (3)$$

What follows is a description of the basic components of the CVFF, including how the force field has been altered to account for chemical reactivity.

The potential energy for stretching a covalent bond is represented by a Morse function,

$$V_{\text{bond}} = D[1 - \exp(-\alpha(r - r_e))]^2 \quad \alpha = \sqrt{k_b/(2D)}, \quad (4)$$

where D is the bond dissociation energy, r the distance between the bonded atoms, r_e the equilibrium bond length, and k_b is the force constant. The potential energy term associated with changing the bond angle, θ , between adjacent atoms a, b, c is

$$V_{\text{angle}} = S(ab)S(bc)k_\theta(\theta - \theta_e)^2, \quad (5)$$

where θ_e is the equilibrium angle, k_θ is the angular force constant, and $S(ab)$ and $S(cd)$ are switching functions, which are defined below. Rotations about covalent bonds are restricted by torsional potentials of the form

$$V_{\text{torison}} = S(ab)S(bc)S(cd)k_\phi[1 + \cos(n\phi - \phi_e)]. \quad (6)$$

The dihedral angle, ϕ , is defined by the three bonds between four adjacent atoms: a, b, c , and d (planes abc and bcd). Parameters k_ϕ , n , and ϕ_e determine the height, multiplicity, and position of the barrier to internal rotation. The switching functions, S , are fractional bond orders defined by the following expression

$$S = \begin{cases} 1 & r \leq r_e \\ 1 - \frac{V_{\text{bond}}}{D} & r > r_e. \end{cases} \quad (7)$$

The purpose of these switching functions is to simulate the decay of the bending and twisting forces as the covalent bonds are stretched. The nonbond term (V_{nonbond}) is equal to the sum of the Lennard–Jones 6–12 and Coulomb potentials as defined in Refs. [16,17].

Chemical reactions are modeled in MD_REACT by the following algorithm. After every time step of molecular dynamics, fractional bond orders are computed for every covalent bond in the system. The bond orders are compared

with a pre-defined bond-dissociation criterion (*BDC*). If a fractional bond order, *S*, is less than or equal to *BDC*, the bond is eliminated (i.e. the information about the covalent connection is erased from the database) and the atoms that had been connected by the eliminated bond are labeled as chemically active.

At the next stage, a set of possible bonds is generated, consisting of all possible covalent interactions between the chemically active atoms. Bonds with the largest value of $[D - V_{\text{bond}}]$ (where *D* is the bond dissociation energy) are retained. The maximum number of bonds for each atom is determined by the rules of atomic valence. If the total number of bonds to an atom is equal to its valence and if the fractional bond order of each of its bonds is higher than *BDC*, the chemically active label is removed from the atom. If an atom retains its chemically active status, it is allowed to form one hypervalent bond. Thus, the maximum number of covalent bonds for a chemically active atom is equal to valence + 1. This feature is introduced to describe chemical reactions that occur via hypervalent transition states (for example, H-atom transfer reactions). Once the bond analysis is complete and the structural information is updated, the next time step of molecular dynamics is executed.

It should be noted that, as the result of the bond-breaking/bond-making routine, the bonds between atoms are not formally removed unless they are replaced by new more energetically favorable bonds. For the purpose of quantifying chemical events, a covalent bond between atoms is considered to be broken when its energy is within *kT* of the dissociation energy, where *k* is the Boltzmann constant. The only role of the bond-dissociation criterion is that it determines whether covalently bonded atoms are eligible to participate in chemical reactions. In the simulations reported in this paper, *BDC* has been set to 0.7, which means that an atom is labeled as chemically active when the energy of at least one of its bonds is equal to or higher than 0.3*D*. Because bonds are not replaced unless there are new more energetically favorable bonds, the simulations should be insensitive to the value of *BDC* as long as the activation energies for all reactions are greater than $(1 - BDC)D$. However, if the value of *BDC* is too large, the computational effort involved in examining all of the bonding possibilities becomes excessive. The value of 0.7 was based on the assumption that none of the important elementary reactions have energy barriers less than 0.3*D*, which is about 100 kJ mol⁻¹ for the backbone C–C bonds and about 125 kJ mol⁻¹ for the C–H bonds in the PMMA (see Section 2.2 for information on the bond dissociation energies).

The atom types of chemically active atoms are updated during every bond-breaking/bond-making procedure to reflect the new arrangement of covalent bonds (see Appendix A and Ref. [17] for information on the atom types used in the CVFF force field). When the ‘chemically active’ label is removed from an atom, the types of the

atoms adjacent to the former chemically active atom are also updated. The chemically active label does not itself alter properties of the atoms. The only exception is in the case of sp³-hybridized carbons, which assume the sp² geometry (planar geometry of the radical) when chemically active.

In the present version of MD_REACT, only homogeneous bond dissociation is permitted (i.e. no ions are formed). Partial charges on the atoms participating in breaking and making of covalent bonds are adjusted accordingly. The method is designed to model any chemical reaction involving σ and/or π bonds, with the exception of triple bonds and π conjugated and aromatic systems (which we intend to include in the near future). The energies of π bonds are calculated using the Morse potential (Eq. (4)) of the corresponding double bond with the dissociation energy equal to the difference between dissociation energies of the double bond and the corresponding single (σ) bond.

The RMD algorithm is implemented as a Fortran/C computer code (MD_REACT program) interfaced with Discover 95, which is commercially available molecular dynamics software offered by Accelrys Inc. (formerly, Molecular Simulations Inc.). The function of the MD_REACT program is to compute the reactive force field, while Discover 95 updates the molecular geometry on the basis of the solution of the equations of motion. A separate computer program, called Molecview, has been developed to visualize the results of the MD_REACT simulations in three dimensions.

2.2. Calibration of the force field

The set of the force-field parameters used in the present work was based on version 2.3 of the CVFF provided by Accelrys Inc. As an attempt to improve the parametric description of reactive potential energy surfaces, dissociation energies (*D*) and equilibrium bond lengths (*r_e*) used in the force field were modified on the basis of results obtained from high-level quantum chemical calculations performed on small model compounds. What follows is a brief description of the results of the quantum chemical calculations and how these results were used to obtain the new force-field parameters.

Energetics for the reactions of model compounds was calculated using the CBS-QB3 method [18–21] as implemented in the Gaussian 98 computational chemistry package [22]. CBS-QB3 is a hybrid approach consisting of a series of density-functional and ab initio calculations that are used to determine the geometry of the molecule and to extrapolate the energy of the molecule at this geometry to the complete basis set limit [18–20]. The mean absolute deviation of the ΔH^0 (*T* = 0 K) values computed using this method from the experimental values is less than 4.2 kJ mol⁻¹ [21].

The energy differences between products and reactant were obtained for the set of bond dissociation and β -scission

reactions shown in Table 1. The model reactions were selected to represent chemical transformations of importance in the thermal decomposition of poly(methyl methacrylate). Every reactant molecule was represented by its lowest energy conformation. The geometries of the products were obtained by dividing the reactant molecule into the fragments of interest and optimizing the structures of each of the fragments. Although experimental reaction enthalpies are available for a few of the model reactions given in Table 1, many of the required values have not been measured. In some cases, even when there are experimental values, they have not been critically evaluated so the accuracies of this data are unknown. By using the CBS-QB3 method to compute all of the reaction enthalpies used in the force field, we have reasonable assurance that the errors will be both small and uniform across the reaction set.

The energy differences between the products and reactants obtained for the dissociation reactions, reactions 1–5 and 13–26 in Table 1, were assigned to the corresponding bond dissociation energies (D) in the CVFF force field. In order to provide a first-order correction for quantum effects, the energy differences were corrected for zero-point energy contributions; i.e. the D parameters were set equal to the ΔH^0 ($T = 0$ K) of the corresponding reactions. Computed enthalpies of the β -scission reactions, reactions 6–12 in Table 1, were used to determine the energies of π bonds. The π bond energies were calculated by subtracting the ΔH^0 ($T = 0$ K) of the β -scission reaction from the energy of the σ bond broken as a result of this process. Bond dissociation energies of the σ bonds in the radical reactants were assumed to be equal to those in the corresponding non-radical species. The D parameters for double bonds were set to be equal to the sums of energies of the corresponding σ and π bonds. Equilibrium bond length (r_e) parameters were obtained directly from the optimized structures of the reactants and products.

The set of the Morse parameters determined from the quantum chemical calculations was expanded by performing a series of simple linear extrapolations to account for different atom types. For example, the energy of the bond between C, an sp^3 carbon attached to four non-hydrogens, and C3, an sp^3 carbon attached to three hydrogens and one non-hydrogen, was computed as

$$D(C-C3) = D(C-C2) + D(C2-C3) - D(C2-C2), \quad (8)$$

where C2 is the sp^3 carbon attached to two hydrogens and two non-hydrogens. A full list of the Morse parameters used in these simulations, together with the information on how these parameters were obtained, is provided in Appendix A.

3. Analysis of the thermal decomposition of PMMA

3.1. Simulation setup

The majority of the simulations were performed on a

model of PMMA consisting of the single 15-unit polymer chain displayed in Fig. 1. In order to examine possible inter-chain reactions, several additional simulations were performed on four chains, each consisting of 15 monomer units. The chains were terminated by an H atom at one end and a CH_3 group at the other end. Thus, each single-chain calculation involved about 230 atoms and each four-chain simulation involved 920 atoms. Every molecular dynamics trajectory was computed using periodic boundary conditions. An atom-based summation method [17] with a cutoff of 16.5 Å was used to calculate the nonbond interactions.

The initial model structures were obtained via simulated annealing. An iterative procedure was carried out, beginning with a molecular dynamics calculation at 600 K and a constant pressure of 101 kPa (1 atm), followed by an energy minimization terminated when the maximum derivative was less than $4 \text{ J mol}^{-1} \text{ \AA}^{-1}$. In the succeeding iterations, the temperature was decremented by 10° and the process repeated until the specified temperature for the dynamics was 0 K.

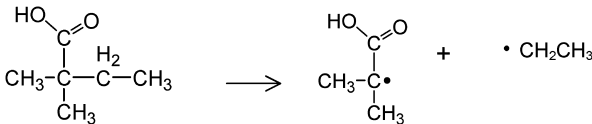
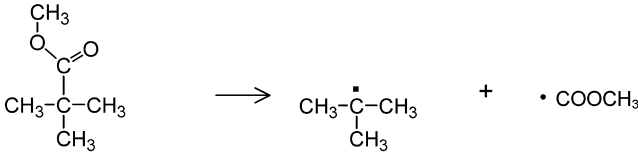
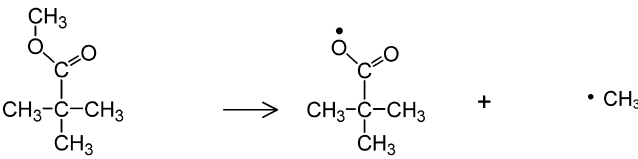
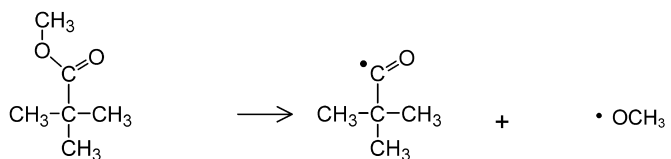
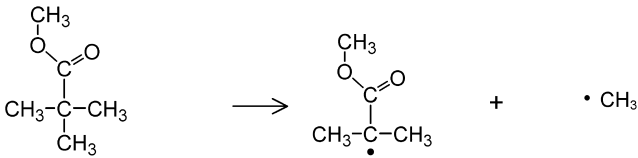
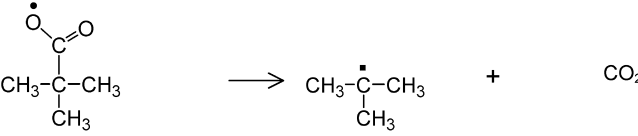
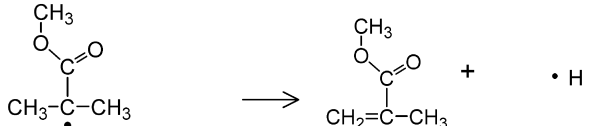
Simulations were performed at 1000, 1200, and 1500 K. The value of 1000 K as the lowest temperature was dictated by the necessity to observe reactive events within computationally feasible simulation times. In order to accumulate statistics on chemical reactions, 10 single-chain and 3 four-chain simulations were done at every temperature.

Each simulation was carried out in two stages. In the first stage, the structure was equilibrated by molecular dynamics. Thermal motion was initiated by giving each atom a three-dimensional velocity chosen at random from the Maxwell–Boltzmann distribution. The dynamics was performed at constant pressure (101 kPa) and temperature (NPT ensemble). In order to avoid dissociation of covalent bonds at the equilibration stage, the Morse term (Eq. (4)) in the CVFF was temporarily replaced by the corresponding harmonic potential ($r_e^{\text{harmonic}} = r_e^{\text{Morse}}$, $k_b^{\text{harmonic}} = k_{\text{Morse}}^b$). The time of the equilibration dynamics varied between 0.5 and 15 ps. The average density of the equilibrated PMMA systems showed a weak temperature dependence decreasing from 1.04 to 1.02 g cm^{-3} with the increase of temperature.

In the second stage, RMD was performed starting with the structure and velocity distribution generated in the equilibration procedure. The dynamics was carried out at constant volume and temperature (NVT ensemble). The time of the RMD varied between 2 and 100 ps.

The Verlet velocity algorithm [23,17] was used in the integration of Hamilton's equations (Eq. (1)). The integration time step varied between 1 and 0.2 fs (smaller time steps were used at higher temperatures in order to avoid divergence). The Andersen pressure control method [24] and direct velocity-scaling temperature control algorithm

Table 1
CBS-QB3 enthalpies of the reactions representing decomposition of PMMA

No.	Reaction	$\Delta H^0 (T = 0 \text{ K}), \text{ kJ mol}^{-1}$
1		329 (358)
2		383 (406)
3		364 (395)
4		420 (448)
5		332 (364)
6		-72 (-60)
7	$\cdot\text{COOCH}_3 \rightarrow \text{CO}_2 + \cdot\text{CH}_3$	-92 (-72)
8		174 (198)

(continued on next page)

Table 1 (continued)

No.	Reaction	ΔH^0 ($T = 0$ K), kJ mol^{-1}
9	$\begin{array}{c} \text{HC}=\text{O} \quad \text{HC}=\text{O} \\ \quad \\ \text{CH}_3\text{CH}-\text{C}-\dot{\text{C}}\text{H} \\ \\ \text{H}_2 \end{array} \longrightarrow \begin{array}{c} \text{HC}=\text{O} \\ \\ \text{CH}_3-\dot{\text{C}}\text{H} \end{array} + \begin{array}{c} \text{HC}=\text{O} \\ \\ \text{H}_2\text{C}=\text{CH} \end{array}$	97 (112)
10	$\begin{array}{c} \text{CH}_3 \\ \\ \text{O} \\ \\ \text{C}=\text{O} \\ \\ \dot{\text{C}}\text{H}_2-\text{C}-\text{CH}_3 \\ \\ \text{CH}_3 \end{array} \longrightarrow \begin{array}{c} \text{CH}_2=\text{C}-\text{CH}_3 \\ \\ \text{CH}_3 \end{array} + \cdot\text{COOCH}_3$	113 (120)
11	$\begin{array}{c} \text{CH}_3 \\ \\ \text{O} \\ \\ \text{C}=\text{O} \\ \\ \dot{\text{C}}\text{H}_2-\text{C}-\text{CH}_3 \\ \\ \text{CH}_3 \end{array} \longrightarrow \begin{array}{c} \text{CH}_3 \\ \\ \text{O} \\ \\ \text{C}=\text{O} \\ \\ \text{CH}_2=\text{C}-\text{CH}_3 \end{array} + \cdot\text{CH}_3$	91 (108)
12	$\begin{array}{c} \text{HO} \\ \\ \text{C}=\text{O} \\ \\ \dot{\text{C}}\text{H}_2-\text{C}-\text{C}-\text{CH}_3 \\ \quad \\ \text{CH}_3 \quad \text{H}_2 \end{array} \longrightarrow \begin{array}{c} \text{HO} \\ \\ \text{C}=\text{O} \\ \\ \text{CH}_2=\text{C} \\ \\ \text{CH}_3 \end{array} + \cdot\text{CH}_2\text{CH}_3$	80 (94)
13	$\begin{array}{c} \text{HC}=\text{O} \quad \text{HC}=\text{O} \\ \quad \\ \text{CH}_3\text{CH}-\text{C}-\dot{\text{C}}\text{H}_2 \end{array} \longrightarrow \begin{array}{c} \text{HC}=\text{O} \\ \\ \text{CH}_3-\dot{\text{C}}\text{H} \end{array} + \begin{array}{c} \text{HC}=\text{O} \\ \\ \dot{\text{C}}\text{H}_2-\text{CH}_2 \end{array}$	334 (361)
14	$\text{CH}_3\text{CH}_3 \rightarrow \cdot\text{CH}_3 + \cdot\text{CH}_3$	370 (410)
15	$\text{CH}_3\text{CH}_3 \rightarrow \cdot\text{CH}_2\text{CH}_3 + \cdot\text{H}$	418 (458)
16	$\text{CH}_3\text{CH}_2\text{CH}_3 \rightarrow \cdot\text{CH}_2\text{CH}_3 + \cdot\text{CH}_3$	366 (404)
17	$\text{CH}_3\text{CH}_2\text{CH}_3 \rightarrow \cdot\text{CH}(\text{CH}_3)_2 + \cdot\text{H}$	406 (446)
18	$\text{CH}_3\text{CH}_2\text{CH}_2\text{CH}_3 \rightarrow \cdot\text{CH}_2\text{CH}_3 + \cdot\text{CH}_2\text{CH}_3$	364 (398)
19	$\begin{array}{c} \text{CH}_3 \\ \\ \text{CH}_3-\text{C}-\text{CH}_2\text{CH}_3 \\ \\ \text{CH}_3 \end{array} \longrightarrow \begin{array}{c} \text{CH}_3 \\ \\ \dot{\text{C}}-\text{CH}_3 \\ \\ \text{CH}_3 \end{array} + \cdot\text{CH}_2\text{CH}_3$	354 (386)
20	$\text{CH}_2=\text{CHCH}_2\text{CH}_3 \rightarrow \cdot\text{CH}=\text{CH}_2 + \cdot\text{CH}_2\text{CH}_3$	411 (444)
21	$\text{CH}_2=\text{CHCH}_2\text{CH}_3 \rightarrow \cdot\text{CH}_2\text{CH}=\text{CH}_2 + \cdot\text{CH}_3$	307 (340)
22	$\text{CH}_2=\text{CHCH}_2\text{CH}_3 \rightarrow \text{CH}_2=\dot{\text{C}}-\text{CH}_2\text{CH}_3 + \cdot\text{H}$	444 (481)
23	$\text{H}_2 \rightarrow \cdot\text{H} + \cdot\text{H}$	437 (463)
24	$\text{CH}_3\text{OH} \rightarrow \cdot\text{OCH}_3 + \cdot\text{H}$	435 (474)
25	$\text{CH}_3\text{OOCH}_3 \rightarrow \cdot\text{OCH}_3 + \cdot\text{OCH}_3$	166 (191)
26	$\text{CH}_3\text{OCH}_2\text{CH}_3 \rightarrow \cdot\text{OCH}_3 + \cdot\text{CH}_2\text{CH}_3$	360 (392)

Difference between energies of the products and reactant are given in parentheses. Zero-point energy contributions are not included.

[17] were used during the annealing and equilibration dynamics.

Both the Nosé–Hoover [25,26,17] and direct velocity-scaling algorithms were considered for controlling the

temperature of the decomposing polymers during the RMD simulations. A series of 20 single-chain PMMA simulations (10 with each temperature control algorithm) was performed at the target temperatures of 1000 and 1500 K. The

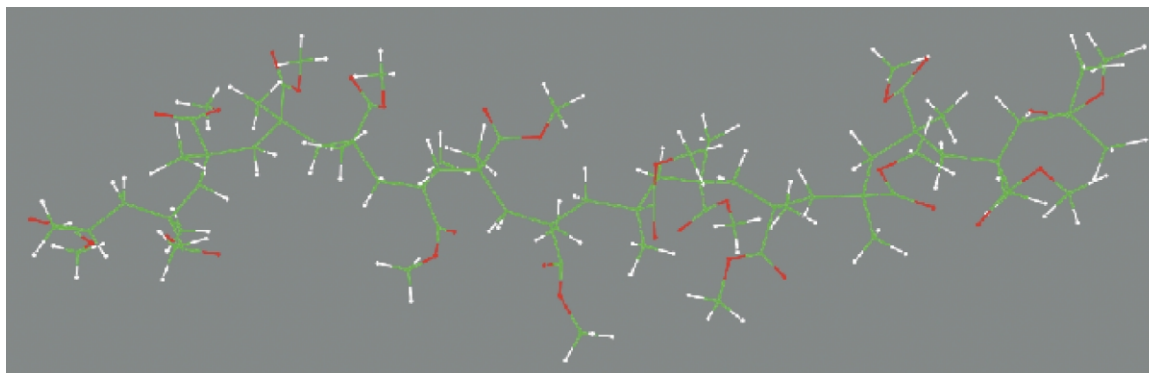


Fig. 1. 15-unit single-chain model of PMMA.

instantaneous temperature fluctuations were confined within the assigned boundaries of ± 10 K in all of the simulations in which direct velocity-scaling was employed. In most of the simulations in which the Nosé–Hoover algorithm was used, however, substantial temperature fluctuations, ranging from $\pm 15\%$ to $\pm 30\%$ of the target temperature, were observed. These fluctuations frequently led to divergence. Reducing the values of the fictitious mass (Q -parameter) and time step did not dampen the magnitude of these fluctuations. On the other hand, when we compared the chemistry and kinetics obtained from the simulations in which direct velocity-scaling was employed to the results of Nosé–Hoover-controlled simulations, we found that the results were essentially identical as long as the temperature fluctuations were $< 20\%$ of the target temperature. On the basis of these observations, we concluded that direct velocity-scaling is better suited than the Nosé–Hoover algorithm for high temperature reactive simulations. Thus, the temperatures of the RMD simulations, which are reported in the ensuing sections of this paper, were controlled by direct velocity-scaling.

3.2. Results and discussion

The total time for each reactive dynamics simulation was

chosen in such way that the degree of conversion would be 20–30%, determined as the ratio of the mass of volatile products versus initial mass of the polymer. Products with masses less than the mass of the dimer were considered to be volatile.

A still frame from a representative simulation is shown in Fig. 2. According to the simulation results, methyl methacrylate (monomer) is the dominant volatile product of the thermal degradation of PMMA. The average mass fraction of monomer (with respect to the total mass of volatile products) decreased from 90 to 80% as the temperature was increased from 1000 to 1500 K. The generation of monomer was accompanied by formation of a number of low-molecular-weight stable species (H_2 , CO , CO_2 , CH_4 , C_2H_4 , C_2H_6 , HCOOCH_3) in trace amounts. Experimental analysis of the volatile products of the decomposition of PMMA, summarized in Ref. [27], indicates that 81–83% of the product is monomer at 1070 K. This value, along with the experimental results of analysis of trace volatile products, is in good agreement with the results of the MD_REACT simulations. At 1470 K, the experimentally determined fraction of methyl methacrylate decreases to about 13%. The decrease is attributed to cracking of the monomer in secondary reactions. Full-scale modeling of such secondary processes would require much longer simulation times and was not the primary goal of this study.

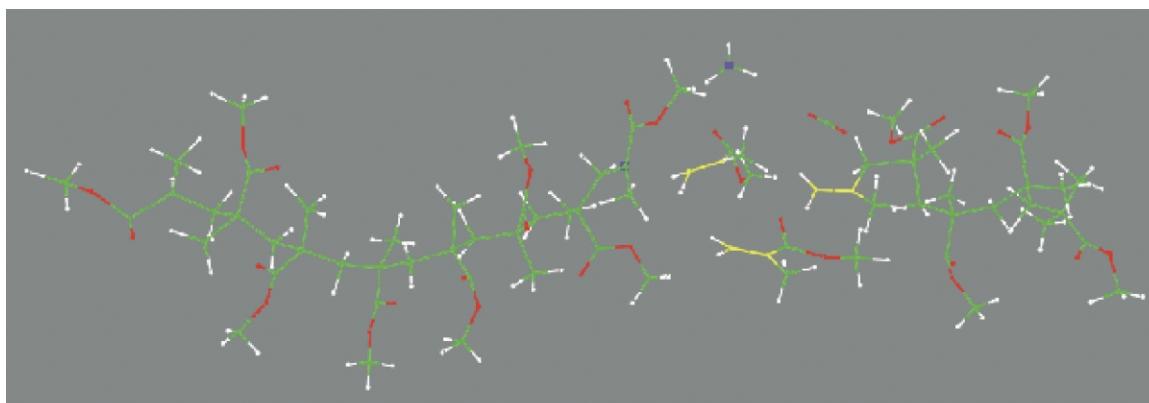


Fig. 2. Still frame from an MD_REACT simulation of the thermal degradation of PMMA: single-chain model after 7.0 ps of reactive dynamics at $T = 1200$ K.

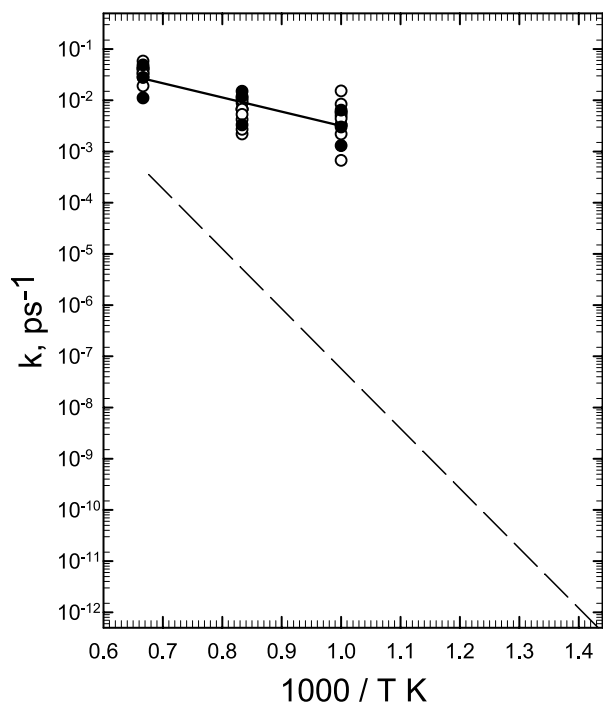


Fig. 3. Temperature dependence of the rate constant of production of monomer (the rate per structural unit of the reacting polymer) in thermal decomposition of PMMA. Empty circles are the results of single-chain simulations; filled circles are the results of four-chain simulations; solid line represents Arrhenius fit of all the data points. The broken line is based on the Arrhenius parameters ($E = 224 \text{ kJ mol}^{-1}$, $A = 2.9 \times 10^{16} \text{ s}^{-1}$) taken from Ref. [28].

The rate constant for the production of methyl methacrylate in the thermal decomposition process was calculated for every simulation using the following expression

$$k = \frac{N_{\text{monomers}}}{N_{\text{units}} t_{\text{sim}}}, \quad (9)$$

where N_{monomers} is the number of monomers formed, N_{units} is the number of structural units in the initial polymer, and t_{sim} is the time of reactive dynamics. The temperature dependence of the calculated rate constant is presented in Fig. 3. The results show a good agreement between the single-chain (empty circles) and four-chain (filled circles) simulations at every temperature. By fitting the temperature dependence with the Arrhenius expression (solid line),

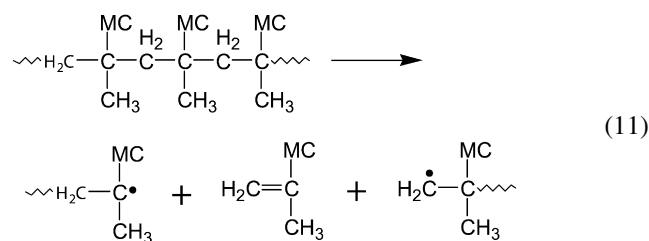
$$k = A \exp\left(-\frac{E}{RT}\right), \quad (10)$$

we obtain a pre-exponential factor $A = (1.9 \pm 2.9) \times 10^{12} \text{ s}^{-1}$ and activation energy $E = 53 \pm 14 \text{ kJ mol}^{-1}$ (uncertainties are given as 2σ ; R is the gas constant).

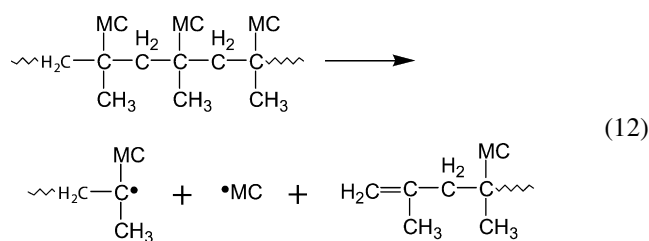
The analysis of distribution of volatile products (discussed earlier) indicates that the reaction corresponding to the formation of monomer accounts for at least 80% of the mass loss in the simulated degradation process. Thus, the Arrhenius parameters obtained from the simulations can be compared with those obtained

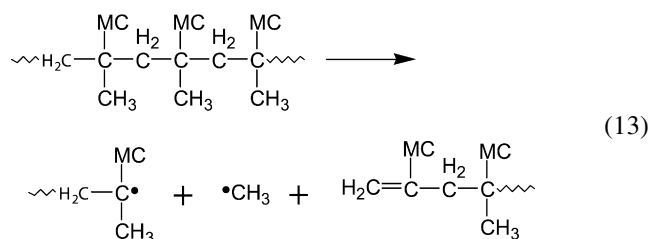
experimentally for the rate constant of the overall mass loss in the thermal decomposition of PMMA. Experimental values of the activation energy between 60 and 270 kJ mol^{-1} have been reported in the literature [12, 15, 27, 28, 29]. The lower values are usually explained by mass transport effects and the presence of weak linkages in the molecular structure of the PMMA sample (unstable end groups, chain defects or irregularities). Taking into account that our PMMA model should not be influenced by either effect, the MD_REACT method appears to underestimate the activation energy for the overall mass loss by at least a factor of 2. It should be noted, however, the experimental measurements were performed at much lower temperatures (500–700 K) than those used in the simulations (1000–1500 K). Therefore, the discrepancy between the computed and experimental activation energy values may be due to the effects of temperature on the kinetics of the decomposition reactions. A more complete discussion of possible sources of this discrepancy is presented at the end of this section.

It has long been accepted that the thermal decomposition of poly(methyl methacrylate) is initiated by random scissions of the polymer backbone [27]. In 1991, Manring suggested an alternative initiation reaction involving scissions of the methoxycarbonyl (MC = COOCH₃) side groups [14]. Manring argued that side-group scission is favored due to a large ‘cage’ recombination effect, which reduces the contribution of the backbone scission. Analysis of the MD_REACT simulations indicates that neither main chain or side group scission is the major initiation channel. In fact, these reactions account for less than 20% of all initiation events. Instead, the major initiation reaction observed in the simulations is Reaction (11)



The branching ratio for this channel is 50–60%. Reactions (12) and (13)



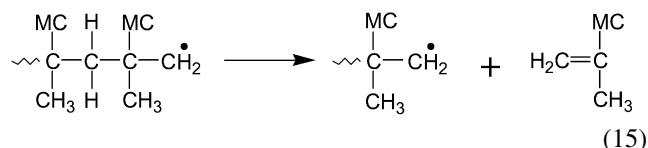
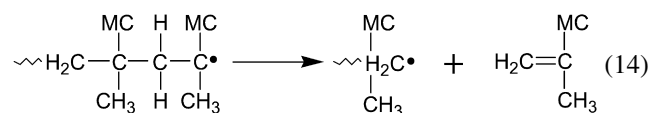


account for a total of 20–25% of all initiations. The branching ratios show no significant temperature dependence within the examined range of temperatures.

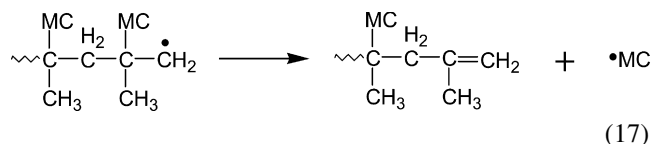
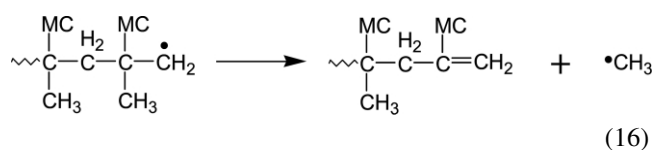
These reactions (Reactions (11)–(13)) may appear improbable because they seem to require two simultaneous bond scissions. However, the two bonds do not really break at the same time. The first scission develops over many time steps. The partially formed radical sites are attached to long and heavy molecular fragments that interact with the surrounding polymer chains. The external and internal interactions and inertia of the fragments prevent the bond from a complete dissociation, at least when it is in the interior of the chain. At some point, the second C–C-bond scission (beta-scission) occurs. The reaction is aided by stabilization of the transition state due to formation of a π bond between the two interior carbons and to a covalent interaction between the two end carbons, which nevertheless eventually become radicals.

It is interesting to note that in addition to the cage recombination effect (which, was emphasized by Manning as playing an important role in the thermal decomposition of PMMA [14]), we also observed the inverse situation, whereby partially dissociated C–C backbone bonds could not be restored. There are a number of factors, which we think may contribute to this phenomenon. These include steric forces arising from non-bonded interactions, the inertia of the heavy polymer fragments, and a potentially large increase in entropy of the system due to the partial bond dissociation. The effect of this phenomenon is that some of the energy of the molecular motion becomes locked in the reaction mode (in form of the potential energy of the bond stretch) for extended periods of time (up to 1 ps) until a further dissociation or β -scission (resulting in Reaction (11), (12), or (13)) occurs. This ‘ratcheting’ effect appears to increase the probability of the initiation reactions by providing a mechanism for the accumulation of energy (over time) in the reaction mode.

Both tertiary and primary macroradicals formed in the initiation process undergo β -scissions to give the monomer, ‘unzipping’ the polymer chains (propagation)



For the tertiary macroradical, Reaction (14) is essentially the only reaction channel observed in the simulations. However, the primary macroradicals also undergo the alternative β -scission reactions



These reactions result in first-order termination of the depolymerization process. This difference in behavior of the tertiary and primary macroradicals was first postulated by Kashiwagi et al. [12]. These authors proposed the β -scission of a pendant MC group in order to provide a mechanistic explanation of the results of their measurements of the molecular-weight distributions of partially degraded PMMA samples.

Our simulations show that Reactions (14) and (15) produce monomers at similar rates. At 1000 K, 2–3 monomers are generated by the primary radical site before termination occurs by Reaction (16) or (17). As the temperature increases, the number of monomers produced by primary macroradicals decreases. At 1500 K, less than 0.5 monomers (on average) are generated by the primary macroradical before termination. Thus, while the rates of Reactions (14) and (15) increase with the increase of temperature, the primary radical channel is effectively shut down by the competing termination reactions. This aspect of the mechanism is one of the factors contributing to the low value of the observed activation energy for the depolymerization process.

Unsaturated end-groups, formed as a result of Reactions (16) and (17), decrease the stability of the newly formed polymer molecules. However, only at higher temperatures (1200–1500 K) were some re-initiation reactions (associated with the scission of C–C backbone bond located in a β position with respect to the terminal double bond) observed. The effect of these reactions is to convert the unsaturated end-groups into tertiary radical sites, which then depolymerize via Reaction (14).

In addition to the depolymerization process, we also observed a number of secondary reactions, which led to formation of the low-molecular-weight species mentioned in the product analysis (see earlier). These reactions include decomposition of methoxycarbonyl radical with either

formation of CO₂ and CH₃ or CO and OCH₃, abstraction of an H atom by small radical species, and recombination of small radicals. At 1500 K, we also observed the formation and destruction of 3- and 4-member-ring cyclic intermediates. According to the simulation results, the secondary reactions have little impact on the overall degradation process.

In Fig. 3, we show Arrhenius extrapolation (broken line) of the PMMA decomposition rate constants, measured by Hirata et al. [28] at 500–700 K, to the temperature range used in the simulations. The simulations overestimate the extrapolated rate constants by 2–5 orders of magnitude. Part of the discrepancy between the simulations and experiment may be attributed to the approximations used in the description of the reactive potential energy surfaces and to uncertainties in the experimental Arrhenius parameters. However, there may be more fundamental reasons for the differences in the values of the rate constants and slopes of these Arrhenius curves.

The complexity of the PMMA decomposition mechanism suggests the possibility of non-Arrhenius behavior of the overall depolymerization rate constant, especially when a wide temperature range (in this case, 500–1500 K) is considered. Some of the factors that can cause non-Arrhenius behavior are changes in the rate-limiting step of the depolymerization process, changes in the chain length of the propagation, and non-Arrhenius behavior of the elementary reaction steps. The initiation reaction, in particular, appears to possess many of the characteristics of reactions that exhibit non-Arrhenius kinetics. The presence of the bulky methyl and MC side groups and the unusual mechanism of this reaction (described earlier) suggest the possibility of a large increase in entropy along the reaction coordinate of the C–C backbone dissociation. This, in turn, would lead to a reduction in the activation energy of this reaction with an increase in temperature [30]. The low activation energy of the initiation reaction together with the decrease in the chain length of the propagation (mentioned earlier) may explain why the activation energy of the simulated decomposition process is much lower than that of the experimental one. It should be noted, however, that a combination of all the factors mentioned above might result in a very complex temperature dependence of the overall depolymerization rate constant. A meaningful analysis of trends of this temperature dependence would require development of a detailed kinetic model of the decomposition process, including detailed kinetic models of all elementary reaction steps, which is beyond the scope of this paper.

4. Concluding remarks

The results of our simulations are in a good overall agreement with the experimentally determined mechanism and product distribution for the thermal decomposition of PMMA. This is the case despite the fact that our dynamically modified force field provides only a first-order approximation to the true potential energy surfaces of

the chemical reactions involved in the thermal decomposition of this polymer. Considerable additional work needs to be done to improve the accuracy of the force field and to provide more rigorous ways of accounting for quantum effects before the quantitative results obtained from the RMD can be used with confidence. The limited time and length scales of the presented methodology are likely to be resolved in the future by advances in the computer technology and by improvements in the efficiency of the RMD algorithm.

The most interesting, if not the most important, observation of this study relates to the effect of the condensed-phase macromolecular environment on the nature of the initiation process. Our simulations suggest that the dynamics of the polymer backbone scission differs substantially from that of bond dissociations in small gas-phase molecules. The nature of this phenomenon and its dependence on the structure and size of polymeric molecules will be explored in more detail in future publications.

Acknowledgements

Partial support for this work was provided by the Federal Aviation Administration (FAA) under an interagency agreement with the National Institute of Standards and Technology (DTFA0003-92-Z-0018) monitored by Dr Richard E. Lyon. Stanislav I. Stoliarov and Phillip R. Westmoreland were supported through Cluster F of the Center for UMass-Industry Research on Polymers, a consortium sponsored by BP/Amoco, US Army, Boeing, CIBA, DuPont, FAA, General Electric, Schneller, Solutia, Titeflex, and Union Carbide. Commercial molecular simulation software used in this work (Cerius [2], Discover, etc.) was granted by Accelrys Inc. (formerly MSI) as a part of the MSI Academic Award 2000 Program.

Appendix A

Table A1
Atom types and Morse parameters used in the CVFF

Atom type	Description
H	Hydrogen atom
Cg	Generic sp ³ carbon
C	sp ³ carbon bonded to 4 heavy atoms
C1	sp ³ carbon bonded to 1 hydrogen and 3 heavy atoms
C2	sp ³ carbon bonded to 2 hydrogens and 2 heavy atoms
C3	sp ³ carbon bonded to 3 hydrogens and 1 heavy atom
C=	Non-aromatic doubly bonded carbon
CC=	sp ³ carbon atom adjacent to C=
C'	Carbon in C=O group
CC'	sp ³ carbon atom adjacent to C'
O	sp ³ oxygen
O'	Oxygen in C=O group

Table A2

No.	Bond	r_e^a (Å)	D (kJ mol ⁻¹)	α^b (Å ⁻¹)	Comment ^c
1	C3–C3	1.53	370	1.915	$D = \Delta H(R14)$
2	C2–C2	1.53	364	1.915	$D = \Delta H(R18)$
3	C2–C3	1.53	366	1.915	$D = \Delta H(R16)$
4	C–C2	1.55	354	1.915	$D = \Delta H(R19)$
5	C–C3	1.55	356	1.915	$r_c = r_c(4)$, $D = D(4) + (D(3) - D(2))$
6	C–C	1.57	344	1.915	$r_c = r_c(4) + (r_c(4) - r_c(2))$, $D = D(4) - (D(2) - D(4))$
7	C1–C3	1.54	361	1.915	Parameters of C1–X bonds are taken to be equal to the average between C2–X and C–X bond parameters
8	C1–C2	1.54	359	1.915	–
9	C1–C1	1.55	354	1.915	–
10	C1–C	1.56	349	1.915	–
11	Cg–C1	1.54	359	1.915	Parameters of Cg–X bonds are taken to be equal to C2–X bond parameters
12	Cg–C2	1.53	364	1.915	–
13	Cg–C3	1.53	366	1.915	–
14	Cg–C	1.55	354	1.915	–
15	Cg–Cg	1.53	364	1.915	–
16	H–C3	1.09	418	1.771	$D = \Delta H(R15)$
17	H–C2	1.10	406	1.771	$D = \Delta H(R17)$
18	H–C1	1.10	395	1.771	$r_c = r_c(17)$, $D = D(17) - (D(16) - D(17))$
19	H–Cg	1.10	406	1.771	$r_c = r_c(17)$, $D = D(17)$
20	CC'–C2	1.55	329	1.915	$D = \Delta H(R1)$
21	CC'–C3	1.54	332	1.915	$D = \Delta H(R5)$
22	CC'–C1	1.56	324	1.915	$r_c = r_c(20) + (r_c(8) - r_c(2))$, $D = D(20) - (D(2) - D(8))$
23	CC'–C	1.57	319	1.915	$r_c = r_c(20) + (r_c(4) - r_c(2))$, $D = D(20) - (D(2) - D(4))$
24	CC'–Cg	1.55	329	1.915	$r_c = r_c(20)$, $D = D(20)$
25	CC'–H	1.10	372	1.771	$D = D(17) - (D(2) - D(20))$
26	C'–CC'	1.53	383	1.915	$D = \Delta H(R2)$
27	C'–Cg	1.53	383	1.915	$r_c = r_c(26)$, $D = D(26)$
28	C'–H	1.11	406	1.771	$D = D(19)$
29	C=C=	1.33	612	2.000	$D = D(15) + [(\Delta H(R13) - \Delta H(R9)) + (\Delta H(R1) - \Delta H(R12)) + (\Delta H(R15) - \Delta H(R8)) + (\Delta H(R5) - \Delta H(R11)) + (\Delta H(R2) - \Delta H(R10))]/5$
30	C=Cg	1.50	412	2.000	$D = \Delta H(R20)$
31	C=C'	1.49	431	2.000	$D = D(30) + (D(27) - D(15))$
32	C=CC'	1.52	377	2.000	$r_c = r_c(30) + (r_c(24) - r_c(15))$, $D = D(30) - (D(15) - D(24))$
33	C=H	1.09	444	1.771	$D = \Delta H(R22)$
34	CC=C=	1.50	412	2.000	$r_c = r_c(30)$, $D = D(30)$
35	CC=C3	1.54	307	1.915	$D = \Delta H(R21)$
36	CC=C2	1.54	305	1.915	$r_c = r_c(35)$, $D = D(35) - (D(13) - D(12))$
37	CC=C1	1.55	300	1.915	$r_c = r_c(35) + (r_c(11) - r_c(13))$, $D = D(35) - (D(13) - D(11))$
38	CC=C	1.56	295	1.915	$r_c = r_c(35) + (r_c(14) - r_c(13))$, $D = D(35) - (D(13) - D(14))$
39	CC=Cg	1.54	305	1.915	$r_c = r_c(36)$, $D = D(36)$
40	CC=C'	1.54	324	1.915	$r_c = r_c(35)$, $D = D(35) + (D(27) - D(13))$
41	CC=CC'	1.56	270	1.915	$r_c = r_c(35) + (r_c(24) - r_c(13))$, $D = D(35) - (D(13) - D(24))$
42	CC=H	1.10	347	1.771	$D = D(19) - (D(15) - D(39))$
43	CC=CC=	1.55	246	1.915	$r_c = r_c(39) + (r_c(39) - r_c(15))$, $D = D(39) - (D(15) - D(39))$
44	C'–C'	1.53	402	1.915	$r_c = r_c(27)$, $D = D(27) + (D(27) - D(15))$
45	CC'–CC'	1.57	295	1.915	$r_c = r_c(24) + (r_c(24) - r_c(15))$, $D = D(24) - (D(15) - D(24))$
46	H–H	0.74	437	1.956	$D = \Delta H(R23)$
47	O–C3	1.42	364	2.000	$D = \Delta H(R3)$
48	O–C2	1.42	360	2.000	$D = \Delta H(R26)$
49	O–C1	1.43	355	2.000	$r_c = r_c(48) + (r_c(11) - r_c(12))$, $D = D(48) - (D(12) - D(11))$
50	O–C	1.44	350	2.000	$r_c = r_c(48) + (r_c(14) - r_c(12))$, $D = D(48) - (D(12) - D(14))$
51	O–Cg	1.42	360	2.000	$r_c = r_c(48)$, $D = D(48)$
52	O–C'	1.35	420	2.000	$D = \Delta H(R4)$
53	O–CC'	1.44	326	2.000	$r_c = r_c(51) + (r_c(24) - r_c(15))$, $D = D(51) - (D(15) - D(24))$
54	O–C=	1.39	408	2.000	$r_c = r_c(51) - (r_c(15) - r_c(30))$, $D = D(51) + (D(30) - D(15))$
55	O–CC=	1.43	301	2.000	$r_c = r_c(51) + (r_c(39) - r_c(15))$, $D = D(51) - (D(15) - D(39))$
56	O–H	0.96	436	2.280	$D = \Delta H(R24)$
57	O–O	1.47	166	1.718	$D = \Delta H(R25)$, α is derived from the corresponding calculated vibrational frequency
58	O'–C'	1.21	815	2.060	$D = D(51) + [(\Delta H(R2) - \Delta H(R6)) + (\Delta H(R3) - \Delta H(R7))]/2$

^a r_e parameters are obtained from the B3LYP/CBSB7 optimized geometries of the model molecules, unless stated otherwise in the Comment section.

^b α parameters are taken from the version 2.3 of the CVFF provided by Accelrys Inc., unless stated otherwise in the Comment section.

^c (R#) is the reference to reaction number in Table 1, (#) is the reference to bond number in this table.

References

- [1] Gardiner WC Jr., editor. *Combustion chemistry*. New York: Springer; 1984.
- [2] Seinfeld JH, Pandis SN. *Atmospheric chemistry and physics*. New York: Wiley; 1998.
- [3] Tuckerman ME, Ungar PJ, von Rosenvinge T, Klein ML. *J Phys Chem* 1996;100:12878–87.
- [4] Car R, Parrinello M. Unified approach for molecular dynamics and density-functional theory. *Phys Rev Lett* 1985;55:2471.
- [5] Nyden MR, Forney GP, Brown JE. *Macromolecules* 1992;25:1658.
- [6] Nyden MR, Coley TR, Mumby S. *Polym Engng Sci* 1997;37:1496.
- [7] Nyden MR. *International Aircraft Fire and Cabin Safety Research Conference*, Atlantic City, NJ; 1998.
- [8] Grassie N, Melville HW. *Proc R Soc A* 1949;190:1.
- [9] Madorsky SL. *J Polym Sci* 1953;11:491.
- [10] Straus S, Madorsky SL. *J Res Natl Bur Stand* 1962;66A:401.
- [11] Kashiwagi T, Inaba A, Brown JE, Hatada K, Kitayama T, Masuda E. *Macromolecules* 1986;19:2160.
- [12] Kashiwagi T, Inaba A, Hamins A. *Polym Degrad Stab* 1989;26:161.
- [13] Manring LE, Sogah DY, Cohen GM. *Macromolecules* 1989;22:4652.
- [14] Manring LE. *Macromolecules* 1991;24:3304.
- [15] Holland BJ, Hay JN. *Polymer* 2001;42:4825.
- [16] Dauber-Osguthorpe P, Roberts VA, Osguthorpe DJ, Wolff J, Genest M, Hagler AT. *Struct Funct Genet* 1988;4:31.
- [17] *Discover 95. User Guide*. San Diego, CA: Biosym/MSI; 1995.
- [18] Petersson GA, Tensfeldt TG, Montgomery Jr. JA. *J Chem Phys* 1991; 94:6091.
- [19] Montgomery Jr. JA, Ochterski JW, Petersson GA. *J Chem Phys* 1994; 101:5900.
- [20] Ochterski JW, Petersson GA, Montgomery Jr. JA. *J Chem Phys* 1996; 104:2598.
- [21] Petersson GA. *Computational thermochemistry: prediction and estimation of molecular thermodynamics*. In: Irikura KK, Frurip DJ, editors. *ACS symposium series*; 1998. Washington, DC.
- [22] Frisch MJ, Trucks GW, Schlegel HB, Scuseria GE, Robb MA, Cheeseman JR, Zakrzewski VG, Montgomery Jr JA, Stratmann RE, Burant JC, Dapprich S, Millam JM, Daniels AD, Kudin KN, Strain MC, Farkas O, Tomasi J, Barone V, Cossi M, Cammi R, Mennucci B, Pomelli C, Adamo C, Clifford S, Ochterski J, Petersson GA, Ayala PY, Cui Q, Morokuma K, Malick DK, Rabuck AD, Raghavachari K, Foresman JB, Cioslowski J, Ortiz JV, Stefanov BB, Liu G, Liashenko A, Piskorz P, Komaromi I, Gomperts R, Martin RL, Fox DJ, Keith T, Al-Laham MA, Peng CY, Nanayakkara A, Gonzalez C, Challacombe M, Gill PMW, Johnson B, Chen W, Wong MW, Andres JL, Head-Gordon M, Replogle ES, Pople JA. *GAUSSIAN 98, Revision A.9*. Pittsburgh, PA: Gaussian, Inc.; 1998.
- [23] Verlet L. *Phys Rev* 1967;159:98.
- [24] Andersen HC. *J Chem Phys* 1980;72:2384.
- [25] Nosé S. *J Chem Phys* 1984;81:511.
- [26] Hoover WG. *Phys Rev* 1985;31:1695.
- [27] Madorsky SL. *Thermal degradation of organic polymers*. New York: Interscience Publishers; 1964.
- [28] Hirata H, Kashiwagi T, Brown JE. *Macromolecules* 1985;18:1410.
- [29] Lomakin SM, Brown JE, Breese RS, Nyden MR. *Polym Degrad Stab* 1993;41:229.
- [30] Gilbert RG, Smith SC. *Theory of unimolecular and recombination reactions*. Oxford: Blackwell; 1990.